

Superior energy-storage properties in (Pb,La)(Zr,Sn,Ti)O₃ antiferroelectric ceramics with appropriate La content

Y Dan, K Zou, G. Chen, Y Yu, Y Zhang, QF Zhang, Y Lu, Q Zhang, Y. He

Abstract

Antiferroelectric (AFE) ceramics based on Pb(Zr,Sn,Ti)O₃ (PZST) have shown great potential for applications in pulsed power capacitors because of their fast charge-discharge rates (on the order of nanoseconds). However, to date, it has been proven very difficult to simultaneously obtain large recoverable energy densities W_{re} and high energy efficiencies η in one type of ceramic, which limits the range of applications of these materials. Addressing this problem requires the development of ceramic materials that simultaneously offer a large ferroelectric-antiferroelectric (FE-AFE) phase-switching electric field E_A , high electric breakdown strength E_b , and narrow polarization-electric field (P - E) hysteresis loops. In this work, via doping of La³⁺ into (Pb_{1-1.5x}La_x)(Zr_{0.5}Sn_{0.43}Ti_{0.07})O₃ AFE ceramics, large E_A and E_b due to respectively enhanced AFE phase stability and reduced electric conductivity, and slimmer hysteresis loops resulting from the appearance of the relaxor AFE state, are successfully obtained, and thus leading to great improvement of the W_{re} and η . The most superior energy storage properties are obtained in the 3 mol% La³⁺-doped (Pb_{1-1.5x}La_x)(Zr_{0.5}Sn_{0.43}Ti_{0.07})O₃ AFE ceramic, which simultaneously exhibits at room temperature a large W_{re} of 4.2 J/cm³ and a high η of 78%, being respectively 2.9 and 1.56 times those of (Pb_{1-1.5x}La_x)(Zr_{0.5}Sn_{0.43}Ti_{0.07})O₃ AFE ceramics with $x = 0$ ($W_{re} = 1.45$ J/cm³, $\eta = 50\%$) and also being superior to many previously published results. Besides, both W_{re} and η change very little in the temperature range of 25–125 °C. The large W_{re} , high η , and their good temperature stability make the Pb_{0.955}La_{0.03}(Zr_{0.5}Sn_{0.43}Ti_{0.07})O₃ AFE ceramic attractive for preparing high pulsed power capacitors useable in various conditions.

Keywords

Relaxor antiferroelectrics, La³⁺ content, Energy-storage density, Energy efficiency,
Temperature stability

1. Introduction

In recently, much attention and research interest has been devoted to energy-storage devices in order to meet the needs of social sustainable development [1,2]. Present energy-storage devices mainly consist of electrochemical capacitors, batteries, dielectric capacitors and fuel cells. In all these energy-storage devices, dielectric capacitors have faster charge-discharge rate ($<1 \mu\text{s}$), more excellent fatigue endurance, and lower energy loss, and thus are widely used in electromagnetic guns, particle beam accelerators, laser technology, and hybrid electrical vehicles, which require a rapid and gigantic energy release so as to acquire large pulsed power [3,4]. Dielectric materials used in dielectric capacitors are classified into four categories: ferroelectrics (FEs), linear dielectrics (LDs), antiferroelectrics (AFEs), and relaxor ferroelectrics (RFEs). Generally, AFEs can exhibit more superior energy-storage properties than FEs because of their near-zero remnant polarization, and than LDs and RFEs due to their larger saturation polarization [5,6]. Thus, in recent years, energy-storage properties of AFE materials, especially $(\text{Pb,La})(\text{Zr,Sn,Ti})\text{O}_3$ AFE systems on account of their wide AFE phase region, have been widely studied and reported [[7], [8], [9], [10], [11]].

For AFE materials, as presented in Fig. 1, the total energy-storage density (W), the recoverable energy-storage density (W_{re}), and the energy efficiency η can be respectively defined as [12]: (1) $W = W_{\text{re}} + W_{\text{loss}} = \int_0^{P_{\text{max}}} E dP$ (upon charging), (2) $W_{\text{re}} = -\int_{P_{\text{max}}}^{P_{\text{r}}} E dP$ (upon discharging), (3) $\eta = \frac{W_{\text{re}}}{W} \times 100\%$, where the P_{max} and P_{r} are respectively the maximum and the remnant polarization, and the E is the applied external electric field. From Fig. 1 and Eqs. (1), (2), it is clear that increasing E_{A} , the electric breakdown strength (E_{b}), P_{max} , and decreasing the electrical hysteresis ($\Delta E = E_{\text{F}} - E_{\text{A}}$) improve W_{re} and η , respectively. Thus, AFEs which exhibit high E_{A} , E_{b} , P_{max} and slim double P-E hysteresis loops are best choice for developing and preparing dielectric capacitors possessing superior energy-storage properties.

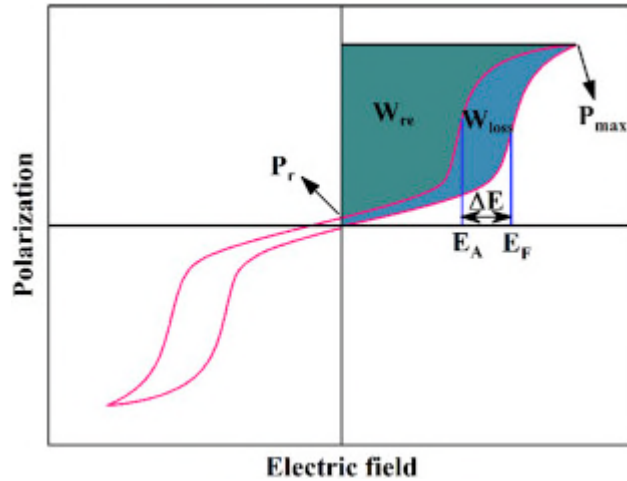


Fig. 1. Schematic diagram showing energy-storage properties of AFE materials.

In $(\text{Pb,L a})(\text{Zr,S n,T i})\text{O}_3$ AFE materials, the contents of Zr, Ti, Sn, and La all have obvious effects on E_A , P_{max} , E_b , and ΔE [9,11,13,14]. For example, upon continuously increasing the La^{3+} content, the phase structure of $(\text{Pb,L a})(\text{Zr,S n,T i})\text{O}_3$ ceramics at room temperature transforms from AFE state to relaxor AFE state with slimmer hysteresis loops, larger E_A , and higher E_b [15,16]. This is good for improving W_{re} and η . However, to date, only two research groups have reported how the La^{3+} content affects energy-storage characteristics of $(\text{Pb,L a})(\text{Zr,S n,T i})\text{O}_3$ AFE ceramics. Because of inappropriate Zr:Sn:Ti ratios, the maximum W_{re} is only 1.47 J/cm^3 , which is far less than that required for practical applications of dielectric capacitors [13,17]. Very recently, we found that $(\text{Pb,L a})(\text{Zr,S n,T i})\text{O}_3$ AFE ceramics with high Sn content have a superior energy-storage capacity because the introduction of elemental Sn can make the P-E hysteresis loops slimmer and increase E_b [11]. Thus, adding more La^{3+} into these AFE ceramics with high Sn content may lead to a larger W_{re} and a higher η .

Based on above discussion, in this work, we study the influence of the La^{3+} content on the phase structure, surface morphology, and energy-storage characteristics of $(\text{Pb}_{1-1.5x}\text{La}_x)(\text{Zr}_{0.5}\text{Sn}_{0.43}\text{Ti}_{0.07})\text{O}_3$ AFE ceramics with high Sn content. With the optimum La^{3+} content, the ceramic exhibits simultaneously a large W_{re} of 4.2 J/cm^3 and a high η of 78%,

which are respectively 2.9 and 1.56 times greater than those of (Pb_{1-1.5x}La_x)(Zr_{0.5}Sn_{0.43}Ti_{0.07})O₃ AFE ceramics with $x = 0$ ($W_{re} = 1.45 \text{ J/cm}^3$, $\eta = 50\%$) and are also superior to many previously reported results. Furthermore, we attempted to correlate quantitatively the EF, EA, and ΔE with the temperature variation.

2. Experimental procedures

(Pb_{1-1.5x}La_x)(Zr_{0.5}Sn_{0.43}Ti_{0.07})O₃ (PLZST) ($x = 0, 0.5\%, 1\%, 1.5\%, 2.5\%, 3\%, 4\%, 5\%$) AFE ceramics were prepared via the conventional ceramic fabrication technique, using PbO ($\geq 99\%$), La₂O₃ ($\geq 99.99\%$), TiO₂ ($\geq 98\%$), SnO₂ ($\geq 99.5\%$) and ZrO₂ ($\geq 99\%$) as raw materials. These powders were weighed on the basis of above chemical formula, ball milled and calcined at 870 °C for 2 h. The powders were ball milled again, pressed into discs of 1.5 mm thickness and 11.5 mm diameter, and sintered at 1230 °C for 2 h. In order to measuring electrical properties, the sintered ceramics were covered with silver electrodes at 550 °C for 10 min.

The apparent density of the sintered sample was measured by the Archimedes method. The phase and crystal structure of the ceramics were examined by the powder x-ray diffraction (XRD; D8 Advance; Bruker, Karlsruhe, Germany). The micrographs of the fresh ceramics were performed by the scanning electron microscopy (SEM; JSM 6510LV; Jeol, Tokyo, Japan). Elemental mappings were done using a SEM (FE-SEM; SIGMA 500; Zeiss, Oberkochen, Germany). The polarization-electric field (P-E) hysteresis loops were characterized at 10 Hz with a precision ferroelectric measurement system (PolyK Technologies, State College, Pennsylvania, USA).

3. Results and discussion

Fig. 2(a) gives XRD patterns of PLZST ceramics with different La³⁺ contents at the room temperature. The results clearly demonstrate that all ceramics have a pure perovskite structure without secondary or impure phase. To characterize more clearly the phase structure of PLZST ceramics, we examine fine scanning XRD patterns in the 2θ range of 43°–45°, as given in Fig.

2(b). Two split peaks of (200) and (002) are apparently shown, indicating a tetragonal phase structure of the ceramics. In addition, upon increasing the La³⁺ content from x = 0 to x = 5%, both the (200) and (002) peaks shift to higher angles, indicating an decrease in the lattice parameters, as shown in Fig. 3. The decrease of lattice parameters a and c with increasing La³⁺ content in the PLZST ceramics is attributed to smaller ionic radius of La³⁺ (1.36 Å) compared with Pb²⁺ (1.49 Å).

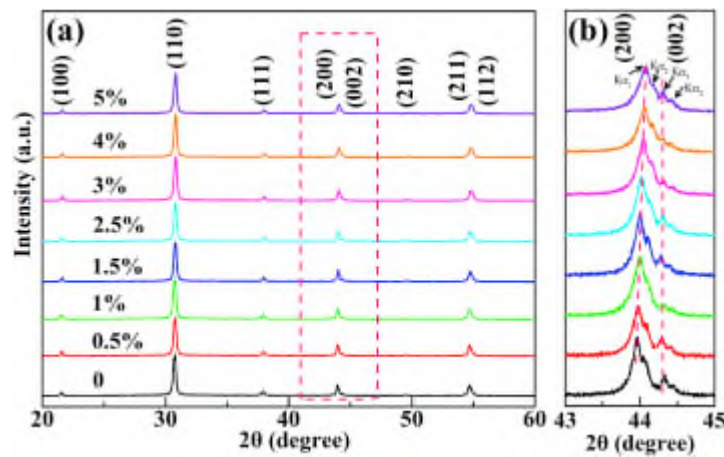


Fig. 2. (a) XRD patterns of PLZST ceramics with different La³⁺ contents. (b) Fine-scan XRD patterns of the PLZST ceramics in 2θ range of 43o-45°; Kα1 and Kα2 indicate the diffraction peaks from Cu Kα1 and Kα2 radiations ($\lambda_{K\alpha1} = 1.5406 \text{ \AA}$ and $\lambda_{K\alpha2} = 1.5444 \text{ \AA}$), respectively.

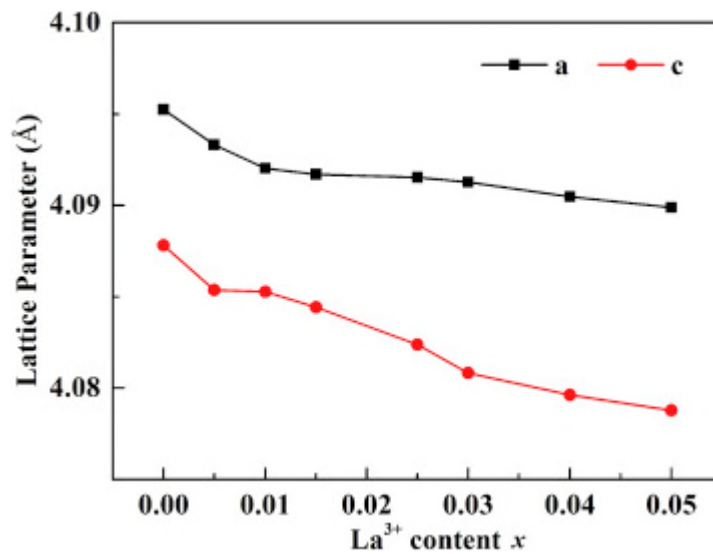


Fig. 3. Lattice parameters a and c of the PLZST ceramics with different La³⁺ contents.

Fig. 4(a)-4(h) show scanning electron micrographs of the fresh PLZST ceramics with various La^{3+} contents. The La^{3+} content distinctly affects the grain size. Upon increasing the La^{3+} content from $x = 0$ to 0.5%, the grain size clearly increases, which may be associated with the higher grain-growth rate caused by quicker diffusion of the smaller La^{3+} ion in place of the larger Pb^{2+} ion. As the La^{3+} content further increases, the ceramic grain size decreases obviously. Introducing additional La^{3+} leads to the formation of Pb^{2+} vacancies with a negative charge, which can be easily segregated at the grain boundary. These vacancies can attract the positively charged La^{3+} ion, thereby creating $\text{La-VPb}''$ pairs near the grain boundary through Columbic interactions. These vacancy-aliovalent ion pairs impede the movement of the grain boundary and thus suppress the grain growth leading to reduced grain size [18,19]. In addition, when the La^{3+} content is less than 3 mol%, all ceramics have a dense microstructure, whereas pores start to appear upon further increasing the La^{3+} content to 4 mol%. Higher La^{3+} content leads to larger lattice distortion and thus more defects in the ceramics.

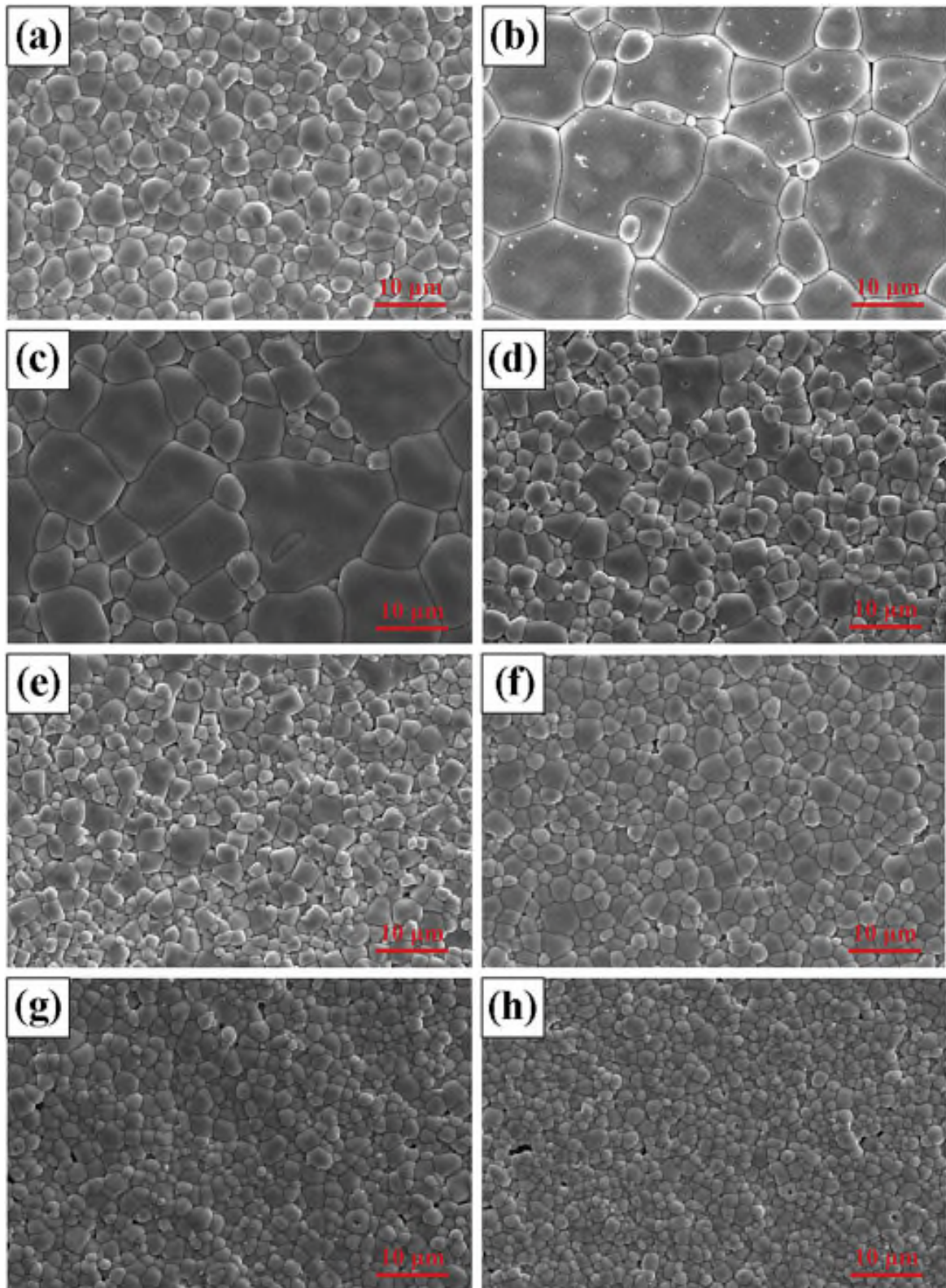


Fig. 4. SEM micrographs of $(\text{Pb}_{1-1.5x}\text{La}_x)(\text{Zr}_{0.5}\text{Sn}_{0.43}\text{Ti}_{0.07})\text{O}_3$ ceramics with different La^{3+} contents: (a) $x = 0$, (b) $x = 0.5\%$, (c) $x = 1\%$, (d) $x = 1.5\%$, (e) $x = 2.5\%$, (f) $x = 3\%$, (g) $x = 4\%$, and (h) $x = 5\%$.

Fig. 5 gives densities of the PLZST ceramics with different La³⁺ contents. As seen from the figure, when the La³⁺ content increases from x = 0 to x = 3%, both apparent and relative densities of the ceramics increase from 7.92 g/cm³ and 92% to 8.25 g/cm³ and 97%, respectively. This means that suitable La³⁺ content benefits the densification of ceramics during the sintering process. However, when the La³⁺ content is beyond 3 mol%, the apparent density and the relative density both decrease obviously, as a consequence of formation of pores in the ceramics as affirmed by the SEM observation.

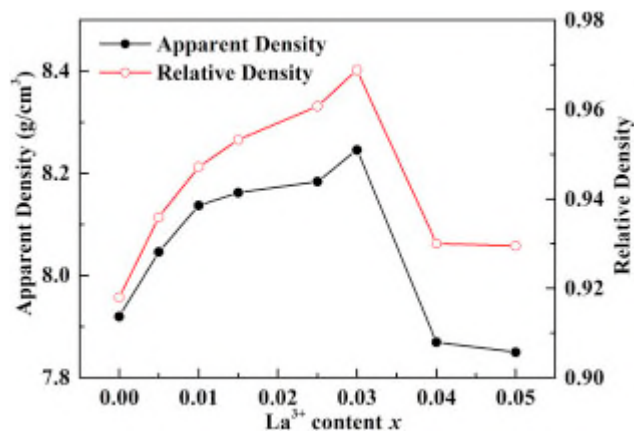


Fig. 5. The apparent density and relative density of the PLZST ceramics with different La³⁺ contents.

Elemental mappings of all ceramics were done using energy-dispersive spectrometry (FESEM/EDS). Fig. 6 displays representative EDS spectra along with a micrograph for the ceramic with x = 3%. All EDS spectra corresponding to various elements were recorded within the same area as in Fig. 6(a). As seen from Fig. 6(b)-6(g), all elements in the PLZST AFE ceramic are detected and evenly distributed without agglomeration. An integrated-area spectrum appears in Fig. 6(h) and is tabulated by atoms and the weight percentage of constituent elements. The atomic ratio given from the area EDS analysis is nearly the same as the stoichiometric formula of the ceramic, which is beneficial for obtaining superior energy-storage properties in this ceramic.

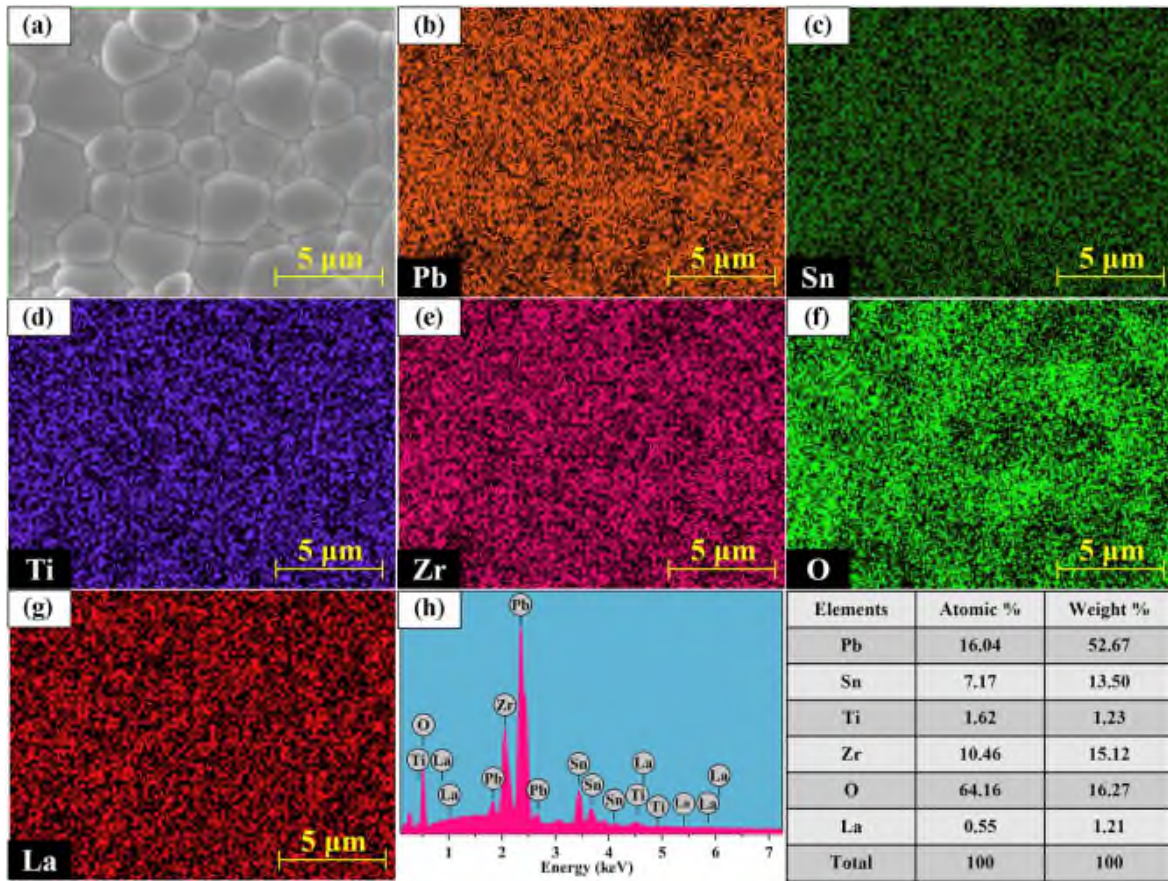


Fig. 6. FESEM-EDS elemental mapping of $(\text{Pb}_{1-1.5x}\text{La}_x)(\text{Zr}_{0.5}\text{Sn}_{0.43}\text{Ti}_{0.07})\text{O}_3$ ceramics with $x = 3\%$: (a) surface microstructure, and elementals mapping of (b) Pb, (c) Sn, (d) Ti, (e) Zr, (f) O, and (g) La. (h) EDS spectrum (left panel) and quantitative atomic and weight percent of various elements (right table).

The La^{3+} content not only affects the microstructure of PLZST AFE ceramics, but also may strongly influence the energy-storage properties. Therefore, it is desirable to find a suitable La^{3+} content for obtaining the best energy-storage characteristics. Fig. 7(a) and (b) show P-E hysteresis loops and current-electric field (I-E) curves, respectively, measured at 10 Hz and room temperature for all ceramics. Fig. 7(c) and (d) present EF, EA, ΔE , W, Wre, and η of the ceramics with various La^{3+} contents, where EF, EA, and ΔE are determined from the I-E curves, and W, Wre, and η are calculated from the P-E hysteresis loops. All ceramics exhibit double P-E hysteresis loops, confirming the AFE symmetry of these ceramics. Besides, as the La^{3+} content increases, E_b first increases and then decreases. Generally, the Pb-based ceramics

exhibit p-type conductivity due to the volatilization of PbO at high sintering temperature. In this study, La³⁺ ions with higher valence substituted for Pb²⁺ ions are considered as donor doping, which neutralizes the hole carriers and thus increases the electric resistivity and breakdown strength of the ceramic. The decrease of the E_b is attributed to the deterioration of the sintering behavior, as affirmed by the SEM observation above. In addition, when the La³⁺ content increases, the shapes of P-E hysteresis loops change from square to slim-slanted and become slimmer, indicating the reduction of the ΔE and thus the increase of the η. Moreover, as seen from Fig. 7(b) and (c), increasing the La³⁺ content clearly improves both E_F and E_A, which is on account of the enhancement of the AFE phase stability. Generally, the stability of the perovskite structure is evaluated by the tolerance factor t, which is expressed as [20]: $t = \frac{r_A + r_O}{\sqrt{2}(r_B + r_O)}$, where r_A, r_B, and r_O are respectively the ionic radii of A-site cation, B-site cation, and oxygen anion. The ferroelectric phase can be stabilized when the tolerance factor is more than 1, and the antiferroelectric phase can be stabilized when the tolerance factor is less than 1. The ionic radius of La³⁺ ions (1.36 Å) is smaller than that of Pb²⁺ (1.49 Å), and thus substitution of La³⁺ for Pb²⁺ in the A-site will suppress the FE state and stabilize the AFE state. The increased E_A, E_b and reduced ΔE contribute to the improved energy-storage properties, as seen in Fig. 7(d). When the La³⁺ content is 3 mol%, the ceramic exhibits optimum energy-storage characteristics, with a large W_{re} of 4.2 J/cm³ and a high η of 78%, which are respectively 2.9 and 1.56 times greater than those of (Pb_{1-1.5x}La_x)(Zr_{0.5}Sn_{0.43}Ti_{0.07})O₃ AFE ceramics with x = 0 (W_{re} = 1.45 J/cm³, η = 50%). Upon further increasing the La³⁺ content to x = 4%, the energy-storage capacity of the ceramic drops because of the decreased E_b.

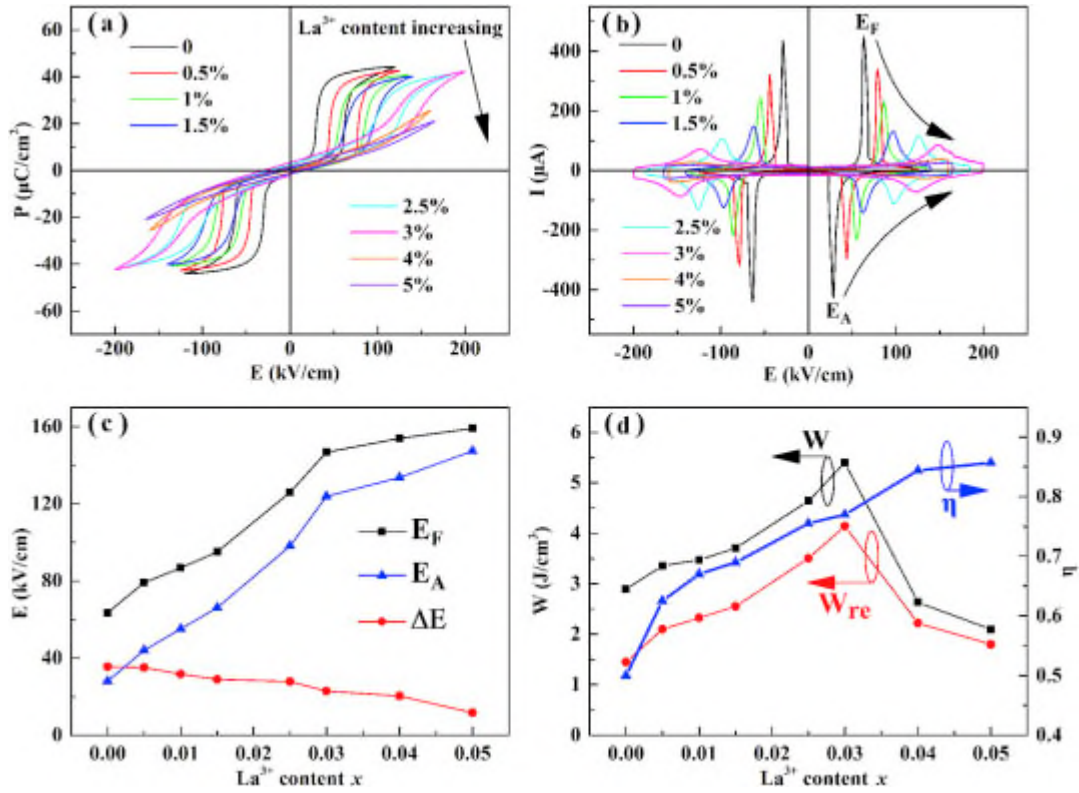


Fig. 7. (a) P-E hysteresis loops, (b) I-E curves, (c) E_F, E_A, ΔE, and (d) W, W_{re}, and η of PLZST ceramics with different La³⁺ contents.

Fig. 8 compares the room-temperature W_{re} and η of recently reported (Pb,La)(Zr,Sn,Ti)O₃ AFE ceramics [[8], [9], [10], [11], [12],[21], [22], [23], [24], [25], [26], [27], [28]]. In previously reported work, it was hardly possible to acquire simultaneously large W_{re} and high η in a single material. For instance, (Pb_{0.858}Ba_{0.1}La_{0.02}Y_{0.008})(Zr_{0.65}Sn_{0.3}Ti_{0.05})O₃- (Pb_{0.97}La_{0.02})(Zr_{0.9}Sn_{0.05} Ti_{0.05})O₃ AFE ceramics possess an excellent W_{re} of 6.40 J/cm³, whereas the η is only about 62.4% [21]. Conversely, Pb_{0.88}La_{0.04}Sr_{0.06}[(Zr_{0.6}Sn_{0.4})_{0.84}Ti_{0.16}]O₃ AFE ceramics have a very high η of 93.3% but suffer from a low W_{re} of 1.52 J/cm³ [22]. In contrast, the Pb_{0.955}La_{0.03}(Zr_{0.5}Sn_{0.43}Ti_{0.07})O₃ AFE ceramic in the present work has simultaneously a very large W_{re} and a fairly high η, which makes it overall superior to other lead-based AFE ceramics in terms of energy-storage properties.

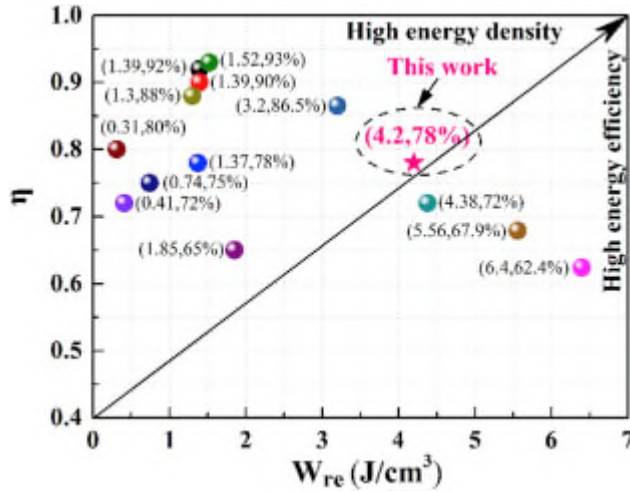


Fig. 8. Comparison of energy densities and efficiencies of recently reported (Pb,La)(Zr,Sn,Ti)O₃ AFE ceramics.

Besides large W_{re} and high η , the temperature stability of the energy-storage characteristics is also of great importance for AFE materials, because dielectric capacitors always have to work over a wide range of temperatures in practical applications. For this reason, we further study in the following the influence of the temperature on energy-storage characteristics for 3 mol% La-doped $(Pb_{1-1.5x}La_x)(Zr_{0.5}Sn_{0.43}Ti_{0.07})O_3$ ceramics (see Fig. 9). As seen in Fig. 9(a), the ceramic exhibits typical double P-E hysteresis loops of AFE materials between 25 °C and 125 °C, and the hysteresis loops become slimmer with increasing measuring temperature. The P_{max} , P_r , $\Delta P = P_{max} - P_r$, EF , EA , and ΔE , which are determined from P-E hysteresis loops and I-E curves [Fig. 9(b)], are presented in Fig. 9(c) as functions of temperature. EF , EA , ΔE , and P_{max} clearly decrease upon increasing the temperature. When the measurement temperature rises, the ceramic transforms from the AFE state gradually to paraelectric (PE) state, and thus the AFE phase stability reduces. This decreases the coupling strength between electric dipoles in the AFE state. In other words, the electric-dipole interaction energy W_{inter} is reduced. In addition, increasing the temperature makes it easier for reorientation of electric dipoles, leading to the decrease of the strain energy W_{str} . Hence, the EF , ΔE and P_{max} , which are respectively proportional to $W_{inter} + W_{str}$, $2W_{str}$ and the stability of AFE phase, reduce with the increase

of the measurement temperature. The reduction of the EA (proportional to $W_{\text{inter}} - W_{\text{str}}$) may be a result of faster decrease of the W_{inter} than the W_{str} [11]. The W , W_{re} , and η measured at 150 kV/cm and different temperature are given in Fig. 9(d). Clearly, in the temperature range of 25–125 °C, the W_{re} exceeds 2 J/cm³, the η is higher than 85%, and their variations are very slight, indicating good temperature stability. These results distinctly make (Pb_{1-1.5x}La_x)(Zr_{0.5}Sn_{0.43}Ti_{0.07})O₃ AFE ceramics with 3 mol% content a potential candidate material for preparing power capacitors that can operate at a high temperature.

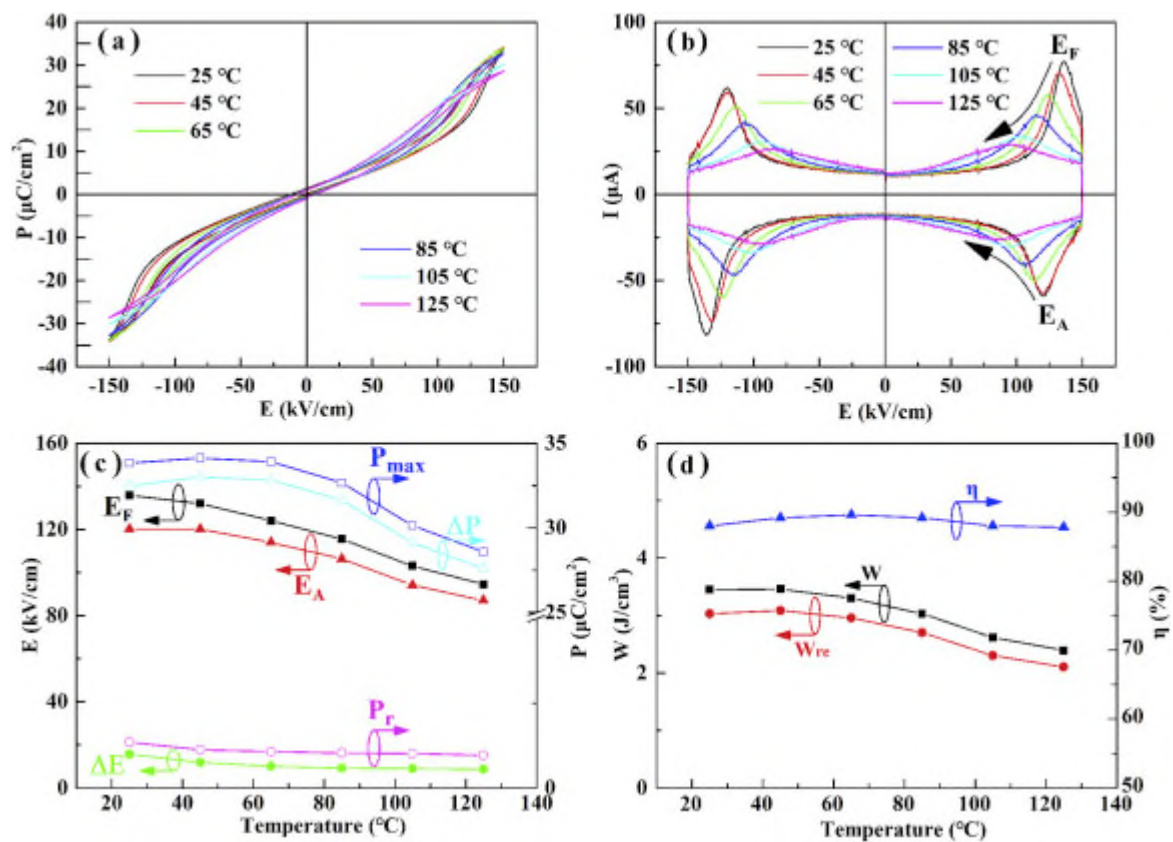


Fig. 9. (a) P-E hysteresis loops measured at 150 kV/cm, (b) I-E curves, (c) E_F , E_A , ΔE , P_{max} , P_r and ΔP , and (d) W , W_{re} , and η of (Pb_{1-1.5x}La_x)(Zr_{0.5}Sn_{0.43}Ti_{0.07})O₃ AFE ceramic with $x = 3\%$ in the temperature range of 25–125 °C.

4. Conclusions

In summary, we prepare (Pb_{1-1.5x}La_x)(Zr_{0.5}Sn_{0.43}Ti_{0.07})O₃ AFE ceramics with different La³⁺ contents in the pure perovskite phase by the traditional ceramic fabrication method, and

then study how the La³⁺ content affects the crystal structure, microscopic morphology, and energy-storage properties of these ceramics. Upon increasing the La³⁺ content, the electric conductivity of the ceramic reduces, the AFE phase stability improves, and the AFE state gradually transforms to the relaxor AFE state with slimmer P-E hysteresis loops, which result in the increase of EA and Eb, and the decrease of ΔE. Thus, the Wre and η improve from 1.45 J/cm³ and 50% (x = 0) to 4.2 J/cm³ and 78% (x = 0.03). However, upon further increasing the La³⁺ content to 4 mol%, the Eb of the ceramic decreases because of the increase of pores, so the Wre reduces to 2.2 J/cm³. Besides, the Wre and η of the ceramic with 3 mol% La³⁺ show good temperature stability between 25 °C and 125 °C. These results indicate the potential of the Pb_{0.955}La_{0.03}(Zr_{0.5}Sn_{0.43}Ti_{0.07})O₃ AFE material for fabricating advanced pulsed capacitors.

Acknowledgments

This work was supported by the NSFC (Nos. 51572073, 51602093, 11774082, 51872079), NSF of Hubei Province (Nos. 2016AAA031, 2018CFB700), Wuhan application foundation frontier Project (No. 2018010401011287), and State Key Laboratory of Advanced Technology for Materials Synthesis and Processing (Wuhan University of Technology; Grant No. 2018-KF-16).

References

- [1] Z.H. Yao, Z. Song, H. Hao, Z.Y. Yu, M.H. Cao, S.J. Zhang, M.T. Lanagan, H.X. Liu Homogeneous/inhomogeneous-structured dielectrics and their energy-storage performances
Adv. Mater., 29 (2017), p. 1601727

[2] Q. Li, L. Chen, M.R. Gadinski, S. Zhang, G.Z. Zhang, H.U. Li, E. Iagodkine, A. Haque, L.Q. Chen, T.N. Jackson, Q. Wang Flexible high-temperature dielectric materials from polymer nanocomposites

Nature, 523 (2015), p. 576

[3] Q. Li, K. Han, M.R. Gadinski, G.Z. Zhang, Q. Wang High energy and power density capacitors from solution-processed ternary ferroelectric polymer nanocomposites

Adv. Mater., 26 (2014), pp. 6244-6249

[4] K. Han, Q. Li, C. Chanthad, M.R. Gadinski, G.Z. Zhang, Q. Wang A hybrid material approach toward solution-processable dielectrics exhibiting enhanced breakdown strength and high energy density

Adv. Funct. Mater., 25 (2015), pp. 3505-3513

[5] B. Li, Q.Y. Liu, X.G. Tang, T.F. Zhang, Y.P. Jiang, W.H. Li, J. Luo Antiferroelectric to relaxor ferroelectric phase transition in PbO modified $(\text{Pb}_{0.97}\text{La}_{0.02})(\text{Zr}_{0.95}\text{Ti}_{0.05})\text{O}_3$ ceramics with a large energy-density for dielectric energy storage RSC Adv., 7 (2017), p. 43327

[6] Z.Q. Hu, B.H. Ma, S.S. Liu, M. Narayanan, U. Balachandran Relaxor behavior and energy storage performance of ferroelectric PLZT thin films with different Zr/Ti ratios

Ceram. Int., 40 (2014), pp. 557-562

[7] Q.F. Zhang, J. Chen, Y.M. Lu, T.Q. Yang, X. Yao, Y.B. He $(\text{Pb},\text{Sm})(\text{Zr},\text{Sn},\text{Ti})\text{O}_3$ Multifunctional ceramics with large electric-field-induced strain and high-energy storage density

J. Am. Ceram. Soc., 99 (2016), pp. 3853-3856

[8] R. Xu, Z. Xu, Y.J. Feng, H.L. He, J.J. Tian, D. Huang Temperature dependence of energy storage in $\text{Pb}_{0.90}\text{La}_{0.04}\text{Ba}_{0.04}[(\text{Zr}_{0.7}\text{Sn}_{0.3})_{0.88}\text{Ti}_{0.12}]\text{O}_3$ antiferroelectric ceramics

J. Am. Ceram. Soc., 99 (2016), p. 2984

- [9] Q.F. Zhang, Y. Dan, J. Chen, Y.M. Lu, T.Q. Yang, X. Yao, Y.B. He Effects of composition and temperature on energy storage properties of (Pb,La)(Zr,Sn,Ti)O₃ antiferroelectric ceramics *Ceram. Int.*, 43 (2017), pp. 11428-11432
- [10] R. Xu, B.R. Li, J.J. Tian, Z. Xu, Y.J. Feng, X.Y. Wei, D. Huang, L.J. Yang Pb_{0.94}La_{0.04}[(Zr_{0.70}Sn_{0.30})_{0.90}Ti_{0.10}]O₃ antiferroelectric bulk ceramics for pulsed capacitors with high energy and power density *Appl. Phys. Lett.*, 110 (2017), p. 142904
- [11] Y. Dan, H.J. Xu, K.L. Zou, Q.F. Zhang, Y.M. Lu, G. Chang, H.T. Huang, Y.B. He Energy storage characteristics of (Pb,La)(Zr,Sn,Ti)O₃ antiferroelectric ceramics with high Sn content *Appl. Phys. Lett.*, 113 (2018), p. 063902
- [12] Q.F. Zhang, H.F. Tong, J. Chen, Y.M. Lu, T.Q. Yang, X. Yao, Y.B. He High recoverable energy density over a wide temperature range in Sr modified (Pb,La)(Zr,Sn,Ti)O₃ antiferroelectric ceramics with an orthorhombic phase *Appl. Phys. Lett.*, 109 (2016), p. 262901
- [13] X. Chen, X. Dong, G. Wang, F. Cao, F. Hu, H. Zhang Dielectric and ferroelectric properties of lanthanum-modified lead zirconate stannate titanate (42/40/18) ceramics *J. Am. Ceram. Soc.*, 101 (2018), pp. 3979-3988
- [14] A.K. Yadav, A. Verma, S. Kumar, V. Srihari, A.K. Sinha, V.R. Reddy, S.W. Liu, S. Biring, S. Sen Investigation of La and Al substitution on the spontaneous polarization and lattice dynamics of the Pb(1-x)LaxTi(1-x)AlxO₃ ceramics *J. Appl. Phys.*, 123 (2018), p. 124102
- [15] P. Liu, D. Zhang Dielectric relaxation of (Pb(1-3x/2)Lax)(Zr_{0.5}Sn_{0.3}Ti_{0.2})O₃ antiferroelectric ceramics induced by lanthanum doping *Acta Phys. Sin.*, 1 (2011), p. 017701
- [16] Y.J. Feng, Z. Xu, H.G. Li, X. Yao Effect of La modifier on the electric hysteresis of lead zirconate stannate titanate compounds *Ceram. Int.*, 30 (2004), pp. 1393-1396
- [17] F.P. Zhuo, Q. Li, Y.Y. Li, J.H. Gao, Q.F. Yan, Y.L. Zhang, X.C. Chu, W.W. Cao Effect of A-site La³⁺ modified on dielectric and energy storage properties in lead zirconate stannate titanate ceramics

Mater. Res. Express, 1 (2014), p. 045501

[18] R.D. Levi, Y. TsurThe effect of oxygen vacancies in the early stages of BaTiO₃ nanopowder sintering Adv. Mater., 17 (2005), pp. 1606-1608

[19] Z. Arif, H. Ali, M. Rizwan Ahmed, M. Adnan, N. Sahn, K. Myong HoDielectric and electromechanical properties of LiNbO₃-modified (BiNa)TiO₃-(BaCa)TiO₃ lead-free piezoceramics

J. Phys. D Appl. Phys., 49 (2016), p. 175301

[20] Y.J. Yu, R.N. SinghEffect of composition and temperature on field-induced properties in the lead strontium zirconate titanate system J. Appl. Phys., 88 (2000), p. 7249

[21] L. Zhang, S.L. Jiang, B.Y. Fan, G.Z. ZhangEnhanced energy storage performance in (Pb_{0.858}Ba_{0.1}La_{0.02}Y_{0.008})(Zr_{0.65}Sn_{0.3}Ti_{0.05})O₃-(Pb_{0.97}La_{0.02})(Zr_{0.9}Sn_{0.05}Ti_{0.05})O₃ anti-ferroelectric composite ceramics by spark plasma sintering

J. Alloy. Comp., 622 (2015), pp. 162-165

[22] R. Xu, Z. Xu, Y.J. Feng, J.J. Tian, D. HuangEnergy storage and release properties of Sr-doped (Pb,La)(Zr,Sn,Ti)O₃ antiferroelectric ceramics Ceram. Int., 42 (2016), pp. 12875-12879

[23] C.H. Xu, Z. Liu, X.F. Chen, S.G. Yan, F. Cao, X.L. Dong, G.S. WangHigh charge-discharge performance of Pb_{0.98}La_{0.02}(Zr_{0.35}Sn_{0.55}Ti_{0.10})_{0.995}O₃ antiferroelectric ceramics

J. Appl. Phys., 120 (2016), p. 074107

[24] Z. Liu, X.F. Chen, W. Peng, C.H. Xu, X.L. Dong, F. Cao, G.S. WangTemperature-dependent stability of energy storage properties of Pb_{0.97}La_{0.02}(Zr_{0.58}Sn_{0.335}Ti_{0.085})O₃ antiferroelectric ceramics for pulse power capacitors Appl. Phys. Lett., 106 (2015), p. 262901

[25] S.E. Young, J.Y. Zhang, W. Hong, X. TanMechanical self-confinement to enhance energy storage density of antiferroelectric capacitors J. Appl. Phys., 113 (2013), p. 054101

- [26] H.L. Zhang, X.F. Chen, F. Cao, G.S. Wang, X.L. Dong Charge-discharge properties of an antiferroelectric ceramics capacitor under different electric fields J. Am. Ceram. Soc., 93 (2010), p. 4015
- [27] I.V. Ciuchi, L. Mitoseriu, C. Galassi Antiferroelectric to ferroelectric crossover and energy storage properties of $(\text{Pb}_{1-x}\text{La}_x)(\text{Zr}_{0.90}\text{Ti}_{0.10})_{1-x}/4\text{O}_3$ ($0.02 \leq x \leq 0.04$) ceramics J. Am. Ceram. Soc., 99 (2016), p. 2382
- [28] R. Xu, Z. Xu, Y.J. Feng, X.Y. Wei, J.J. Tian, D. Huang Polarization of antiferroelectric ceramics for pulse capacitors under transient electric field J. Appl. Phys., 119 (2016), p. 224103